Periventricular white matter abnormalities and restricted repetitive behavior in autism spectrum disorder

Karen Blackmon[a,*], Emma Ben-Avi[a,b], Xiuyuan Wang[a], Heath R. Pardoe[a], Adriana Di Martino[c], Eric Halgren[d,f], Orrin Devinsky[a], Thomas Thesen[a,e], Ruben Kuzniecky[a]

[a]NYU Comprehensive Epilepsy Center, Department of Neurology, New York University School of Medicine, New York, NY 10016, USA
[b]Department of Psychology, New York University, New York, NY 10003, USA
[c]Department of Child and Adolescent Psychiatry, Child Study Center at NYU Langone Medical Center, New York, NY 10016, USA
[d]Department of Radiology, University of California at San Diego, La Jolla, CA 92069, USA
[e]Department of Radiology, New York University School of Medicine, New York, NY 10016, USA
[f]Department of Neurosciences, University of California at San Diego, La Jolla, CA 92069, USA

ARTICLE INFO

ABSTRACT

Malformations of cortical development are found at higher rates in autism spectrum disorder (ASD) than in healthy controls on postmortem neuropathological evaluation but are more variably observed on visual review of in-vivo MRI brain scans. This may be due to the visually elusive nature of many malformations on MRI. Here, we utilize a quantitative approach to determine whether a volumetric measure of heterotopic gray matter in the white matter is elevated in people with ASD, relative to typically developing controls (TDC). Data from a primary sample of 48 children/young adults with ASD and 48 age-, and gender-matched TDCs, selected from the Autism Brain Imaging Data Exchange (ABIDE) open-access database, were analyzed to compare groups on (1) blinded review of high-resolution T1-weighted research sequences; and (2) quantitative measurement of white matter hypointensity (WMH) volume calculated from the same T1-weighted scans. Groupwise WMH volume comparisons were repeated in an independent, multi-site sample (80 ASD/80 TDC), also selected from ABIDE. Visual review resulted in equivalent proportions of imaging abnormalities in the ASD and TDC group. However, quantitative analysis revealed elevated periventricular and deep subcortical WMH volumes in ASD. This finding was replicated in the independent, multi-site sample. Periventricular WMH volume was not associated with age but was associated with greater restricted repetitive behaviors on both parent-reported and clinician-rated assessment inventories. Thus, findings demonstrate that periventricular WMH volume is elevated in ASD and associated with a higher degree of repetitive behaviors and restricted interests. Although the etiology of focal WMH clusters is unknown, the absence of age effects suggests that they may reflect a static anomaly.

1. Introduction

Autism spectrum disorder (ASD) refers to a neurodevelopmental disorder characterized by impairment in social communication and restricted repetitive behaviors and interests (American Psychiatric Association, 2013; Lai et al., 2013; World Health Organization, 1992). Although ASD is a heterogeneous diagnosis with diverse etiologies (Happé et al., 2006; Tuchman et al., 2009), early failures in neuronal genesis, maturation, and migration have been proposed as a root pathological mechanism (Casanova and Casanova, 2014; Ecker and Murphy, 2014). This hypothesis is supported by high rates of developmental malformations in people with ASD on post-mortem neuropathological evaluations (Casanova et al., 2013; Stoner et al., 2014; Wegiel et al., 2010, 2012). Patchy regions of dyslaminated cortex and immature, maloriented neurons, termed "focal cortical dysplasia," are found in up to 91% of ASD brains, relative to 1% of control brains (Stoner et al., 2014). Overproliferation of neurons in the ventricular zone and/or failure to detach and migrate to the cortical zone can result in heterotopic gray matter in the white matter of up to 31% of ASD brains; whereas, no such anomalies were found in age-matched control brains (Wegiel et al., 2010). However, the small sample sizes of these postmortem studies limit generalization to the larger ASD and control population. Detection of morphological abnormalities with in-vivo MRI would allow for more extensive sampling across diverse ASD populations and age ranges. This study aims to determine whether a quantitative marker of heterotopic gray matter on in-vivo MRI (Pardoe et al., 2015) is

* Corresponding author at: NYU Comprehensive Epilepsy Center, Department of Neurology, New York University School of Medicine, 223 East 34th Street, New York, NY 10016, USA.
E-mail address: karen.blackmon@nyumc.org (K. Blackmon).

elevated in children and young adults with ASD, relative to typically developing controls.

Thus far, conventional visual analysis of MRI scans has not resulted in strong evidence for malformations of cortical development as a core finding in ASD (Boddaert et al., 2009; Vasa et al., 2012). This may be due to limitations in MRI-visibility of many malformations (Colombo et al., 2009). Although malformations such as tuberous sclerosis are grossly apparent on visual review, others can be visually elusive, such as periventricular heterotopia and focal cortical dysplasia (Bernasconi et al., 2011; Pascher et al., 2013). Periventricular heterotopia detection is improved with quantitative MRI methods. In people with epilepsy, 46% of heterotopias detected with quantitative MRI were previously overlooked on conventional visual analysis (Pascher et al., 2013).

In the current study, we applied a quantitative approach for detection of periventricular abnormalities in ASD. We segmented and quantified clusters of white matter hypointensity (WMH) on T1-weighted MRI scans using a method that has been validated as a measure of heterotopic gray matter volume in patients with periventricular heterotopia (Pardoe et al., 2015). Children/young adults with ASD were compared to age- and gender-matched typically developing controls (TDCs) on: (1) findings from blinded visual review of high resolution T1-weighted research MRI scans; and (2) WMH volumetric quantification from the same scans. We selected data from the ABIDE repository (Di Martino et al., 2014); for primary analyses we used images acquired from a single scanner and calculated total WMH volume, which included WMH labeled voxels in the periventricular and deep subcortical white matter, as well as the cortical gray–white matter boundary and perivascular spaces. We then removed clusters from the gray–white matter boundary and perivascular spaces to create a WMH-corrected volume of periventricular and deep subcortical white matter clusters only. To evaluate the reliability of our results, we quantified total WMH volume and WMH-corrected volume in an independent, multi-site sample, also selected from the ABIDE repository. We hypothesized that WMH volume would be elevated in ASD, relative to TDCs, in the periventricular and deep subcortical white matter, reflecting failures in neuronal migration (i.e., heterotopia), oligodendrocyte maturation (i.e., dysmyelination), or other processes.

In addition, we tested the hypothesis that elevated WMH volume has early developmental origins by examining the effect of age on WMH-corrected volume. If WMH reflects neurodevelopmental malformations, then WMH volume should not change with age. Rather, these developmental anomalies remain fairly static across the lifespan. This is in contrast to other possible etiological factors for hypointense signal in the white matter such as delayed myelination (Cheng et al., 2010; Lee et al., 2007; Shukla et al., 2011; Wolff et al., 2012), which should show age effects.

Finally, we tested whether elevated periventricular and deep subcortical WMH volume is associated with a loss of functional integrity by performing correlations between WMH-corrected volume and ASD symptom severity on both parent reported and clinician rated symptom measures. Given the location of WMH-corrected clusters in periventricular regions proximal to striatal networks, we hypothesized that elevated WMH-corrected volume would be associated with increased restricted repetitive behaviors, which are subserved by striatal–prefrontal pathways (Langen et al., 2011a,b; Lewis and Kim, 2009).

2. Methods and materials

2.1. Participants

Data were selected from the Autism Brain Imaging Data Exchange (ABIDE) repository (fcon_1000.projects.nitrc.org/indi/abide/). ABIDE is an aggregated and openly shared fully anonymized neuroimaging and phenotypic database that was collected across 17 research sites (Di Martino et al., 2014). All data shared in ABIDE were obtained with

informed consent/assent according to procedures established by the human subjects research board at the respective institutions.

2.1.1. Autism spectrum disorder diagnosis

As detailed elsewhere (Di Martino et al., 2014), acquisition and study protocols varied across each contributing site. Inclusion in the ASD group was based on a DSM-IV-TR clinician diagnosis of Autistic Disorder, Asperger's Disorder, or Pervasive Developmental Disorder not-otherwise-specified. The term ASD is used to specify this broader diagnostic spectrum. Clinical diagnosis varied by sites; it was supported by review of available records and administration of the Autism Diagnostic Observation Schedule (ADOS; Lord et al., 2000) and/or the Autism Diagnostic Interview—Revised (ADI-R; Lord et al., 1994). Comorbid manic or depressive episodes, schizophrenia, traumatic brain injury, genetic syndromes, and epilepsy were generally exclusionary, although specific exclusion criteria varied across sites (see fcon_1000.projects.nitrc.org/indi/abide/).

2.1.2. Typically developing controls

For all samples, inclusion as a TDC required the absence of any current Axis-I disorders or neurological conditions, although procedures for establishing medical and psychiatric history varied across sites (see fcon_1000.projects.nitrc.org/indi/abide/).

2.2. MRI scanning and image processing

For the primary sample, imaging was performed at the New York University Center for Brain Imaging on a 3 T Siemens Allegra head-only MR scanner. Image acquisitions included a T1-weighted volume (TE = 3.25 ms, TR = 2530 ms, TI = 1100 ms, flip angle = 7°, field of view (FOV) = 256 mm, voxel size = $1.3 \times 1.0 \times 1.3$ mm). For the secondary multi-site sample, scanner type and research dedicated MRI sequence parameters differed across sites with details provided as Supplementary material (Appendix Table A.1).

T1-weighted scans from all contributing ABIDE sites were rated for movement artifacts on a scale from 1 (worst quality) to 5 (best quality) by a reviewer blind to group status. The QA ratings may be downloaded from the following site: https://sites.google.com/site/hpardoe/cc_abide (KucharskyHiess et al., 2015). Only scans that received the highest rating (i.e., 4 or 5) were included in this study. Furthermore, scans that were processed were carefully reviewed for FreeSurfersegmentation errors and excluded if errors were detected. This strict approach to scan inclusion was employed to reduce the likelihood that signal intensity abnormalities could be due to motion artifacts, poor image quality, or segmentation errors (Reuter et al., 2015).

For the primary, single-scanner sample, the initial 186 subjects included 79 ASD and 105 TDC. Of these, 48 ASD participants and 94 TDCs met scan inclusion criteria; 48 of the 94 TDCs were case-matched by age (+/− 6 years) and gender to the 48 ASD participants (Table 1). The relatively wide age bracket (6 years) was due to the constraints of TDC data availability; however, 50% of the ASD participants were matched to a TDC within +/− 1.5 year bracket, 33% within +/− 4 year bracket, and 17% within +/− 6 year bracket. T1-weighted scans from the primary sample were reviewed by a board certified neurologist (RK) blind to group status to identify neuroradiologic abnormalities or normal variant findings.

In order to build a similarly sized multi-scanner replication sample, we used the randomize list function in Excel to select subjects from the eight different sites with the largest number of high quality scans based on QA ratings (i.e., rated 4 or 5 as in the primary sample). The resulting replication sample consisted of 80 participants with ASD (69 males/11 females) and 80 TDCs (69 males/11 females) case-matched by age (+/− 6 years), gender, and site to ASD participants (Table 2). For this sample, across sites, 84% of the participants with ASD were matched to a TDC within +/− 1.5 year bracket, 15% within +/− 4 year bracket, and 1% within +/− 6 year bracket.

Table 1
Demographic and neuropsychological data for primary sample.

	ASD		TDC			
Sex ratio	40:8 (males:females)		40:8 (males:females)			
	Mean (SD)	Range	Mean (SD)	Range	t-Value	p-Value
Age at scan (years)	14.15 (5.4)	7–29	14.41 (5.3)	6–29	−0.23	0.82
Handedness[*]	36 (55.2)	−91–95	63.8 (28.5)	−36–100	−3.02	0.003
Full scale IQ[**]	106 (15.5)	76–142	112.2 (13.6)	80–142	−2.11	0.037
Verbal IQ[**]	104.4 (15.2)	74–139	112 (12.7)	85–141	−2.67	0.009
Performance IQ[**]	106.3 (16.1)	72–145	109.9 (14.7)	67–133	−1.13	0.261
ADOS-total	10.8 (4.3)	5–22	–	–	–	–
ADOS-Comm	3.4 (1.6)	0–8	–	–	–	–
ADOS-SI	7.4 (3.2)	2–14	–	–	–	–
ADOS-SBRI	2.3 (1.5)	0–7	–	–	–	–
Gotham-Sev	6.7 (2.3)	3–10	–	–	–	–
Gotham-SA	8.9 (4.3)	3–20	–	–	–	–
Gotham-RRB	3.0 (1.6)	0–7	–	–	–	–
ADI-R social	19 (5.7)	7–28	–	–	–	–
ADI-R verbal	15.5 (4.4)	8–25	–	–	–	–
ADI-R RRB	5.9 (2.7)	0–12	–	–	–	–

ASD = autism spectrum disorder; TDC = typically developing control; SD = standard deviation; IQ = intelligence quotient; ADOS = autism diagnostic observation schedule; Comm = communication; SI = social interaction; SBRI = stereotyped behaviors restricted interests; ADI-R = Autism Diagnostic Inventory—Revised; RRB = restricted and repetitive behaviors.
  [*] Assessed with the Edinburgh Handedness Inventory (Oldfield, 1971); lower scores indicate greater tendency towards left-handedness.
 [**] Assessed with the Wechsler Abbreviated Scale of Intelligence (Wechsler, 1999).

Image files from all sites were transferred to a Linux workstation for morphometric analysis. Images from the primary sample were further processed with the FreeSurfer5.1 software package (http://surfer.nmr.mgh.harvard.edu). Images from the secondary multi-site sample were processed with FreeSurfer 5.3. Processing steps include correction for spatial distortion due to gradient nonlinearity (Jovicich et al., 2006) and B1 field inhomogeneity (Sled et al., 1998). Assignment of a neuro-anatomical label to each voxel is based on a manually labeled training set and Bayesian prior information (Fischl et al., 2002). Labeling is performed by rigid-body alignment of the subject's brain to the probabilistic atlas, followed by non-linear morphing to the atlas. Labels are generated based on the prior probability of a given tissue class occurring at a specific atlas location, the likelihood of the image intensity given that tissue class, and the probability of the local spatial configuration of labels given the tissue class. For the WMH measure, the spatial prior is relaxed to allow for detection of darker voxels anywhere in the white matter. These darker voxels are labeled WMH and summed to quantify total WMH volume. Total supratentorial brain volume (TSBV)

Table 2
Demographic and neuropsychological data for secondary multi-site sample.

	ASD			TDC		
Site	M/F	Mean age (SD) unit: years	Mean IQ (SD)	M/F	Mean age (SD) unit: years	Mean IQ (SD)
PITT	11/2	16.5 (5.6)	107.3 (13.9)	11/2	16.9 (5.7)	108.1 (10.3)
OHSU	6/0	11.3 (2.8)	105 (24.6)	6/0	10.4 (1.4)	117.2 (10.1)
SDSU	4/0	15.0 (1.2)	119.5 (16.8)	4/0	15.2 (1.2)	110.8 (9.6)
USM	14/0	18.8 (5.1)	100.6 (18.9)	14/0	18.7 (5.3)	115.5 (15.1)
CMU	4/1	22.4 (3.1)	112 (8.1)	4/1	22.8 (3.0)	114.2 (8.5)
KKI	7/3	9.9 (1.3)	102.7 (20.5)	7/3	10.2 (1.3)	110.7 (10)
UCLA[*]	20/4	12.5 (2.6)	101.7 (13.5)	20/4	12.4 (1.9)	108 (10.3)
CALTECH	3/1	19.8 (1.6)	109 (13.9)	3/1	19.9 (2.1)	120.5 (10.7)
TOTAL	69/11	14.92 (5.1)	104.6 (16.4)	69/11	14.95 (5.1)	111.5 (11.36)

ASD = autism spectrum disorder; TDC = typically developing control; M/F = male/female; SD = standard deviation; IQ = intelligence quotient; PITT = University of Pittsburgh School of Medicine; OHSU = Oregon Health and Science University; SDSU = San Diego State University; USM = Utah School of Medicine; CMU = Carnegie Melon University; KKI = Kennedy Krieger Institute; UCLA = University of California Los Angeles; CALTECH = California Institute of Technology.
  [*] UCLA samples 1 and 2 combined.

is calculated by summation of all surface-based volumes and labeled voxels inside the pial surface plus any structures that might fall partially or totally outside of the pial surface (e.g., hippocampus, amygdala, corpus callosum, ventral DC, thalamus, ventricles, and choroid plexus), excluding the cerebellum and brain stem.

Following calculation of total WMH volume, we manually removed WMH labeled clusters in the perivascular spaces and re-submitted the images for calculation of remaining WMH volumes. The difference in values between the original WMH volume and the WMH volume after removal of perivascular WMH was retained as a measure of "total perivascular WMH volume."

To quantify WMH subregional volumes for the periventricular region, cortical gray–white matter junction, and deep subcortical white matter, we exported individual WMH masks (Fig. 1A) for further analyses in FSL (http://fsl.fmrib.ox.ac.uk/fsl/fslwiki/), along with ventricle and white matter surface masks generated during FreeSurfer segmentation routines. To calculate periventricular WMH volumes, we dilated the lateral and inferior ventricle masks by 3 mm in every direction (Fig. 1B) and summed WMH-labeled voxels located within the mask. To quantify WMH volume from the cortical gray–white matter junction, we dilated the white matter surface in each direction by 1 mm (Fig. 1C) and summed WMH-labeled voxels within this mask. Deep subcortical WMH volumes were calculated by subtracting periventricular WMH volume and gray–white matter junction WMH volume from the total WMH volume.

2.3. ASD symptom severity

The Autism Diagnostic Observation Scale — Generic (ADOS-G) was administered to all ASD participants in the primary NYU sample. The ADOS-G is a clinician-administered assessment of social interaction, communication, play and imagination (Lord et al, 2000). We examined the relationship between WMH volume and overall ASD symptom severity assessed by the ADOS-G total algorithm score, as well as the *Communication* (*Comm*), *Social Interaction* (*SI*), and *Stereotyped Behaviors and Restricted Interests* (*SBRI*) subscale algorithm scores. The *Communication* subscale assesses both verbal and non-verbal communication. The SI measures elements of social interaction such as eye contact and responsive facial expressions and the SBRI measures repetitive and unusual movements of objects and body and repetitive thoughts about unusual or specific topics. ADOS scores based on a revised algorithm
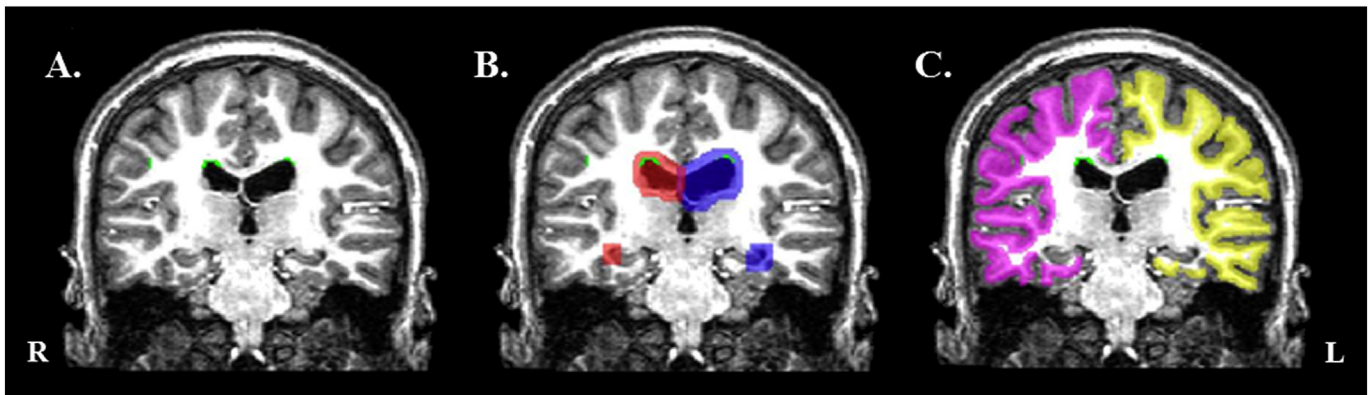
Fig. 1. Calculation of WMH volume from periventricular region and gray–white matter junction. (A) The white matter hypointensity (WMH) mask (green clusters) from a single subject is overlaid on (B) the dilated ventricle masks (red = right lateral and inferior ventricle; blue = left lateral and inferior ventricle) to calculate the total number of WMH voxels that fall within the periventricular region. The WMH mask is overlaid on (C) the dilated white matter surface mask (pink = right hemisphere; yellow = left hemisphere) to calculate the total number of WMH voxels that fall within the gray–white matter junction (GWJ).

(Gotham et al., 2007) were available on 34 of the 48 participants with ASD from the NYU sample. This smaller subset represents the younger participants (below 15 years of age), as the revised algorithm was only available for modules 1–3 at the time of the ABIDE data release and all participants 15 years of age and above were given module 4. The revised algorithm scores include an overall ASD severity scale (*Gotham-Sev*) as well as separate subscales measuring social affect (*Gotham-SA*) and restricted and repetitive behaviors (*Gotham-RRB*) (Gotham et al., 2007).

The ADI-R (Lord et al., 1994) was administered to the majority of ASD participants' parents or caregivers in the primary NYU sample (N = 43). The ADI-R is a semi-structured interview that surveys participants' current behavior across the three domains: reciprocal social interaction (*ADI-R Social*), verbal communication (*ADI-R Verbal*), and restricted, repetitive behaviors (*ADI-R RRB*). Scores from these three indices were correlated with WMH volume to establish convergent validity of findings across symptom inventories based on clinical observation (ADOS) and parent report (ADI-R). ADOS and ADI-R scores were not consistently available across sites for the secondary multi-site sample; therefore, symptom correlations were not run in the secondary sample

2.4. Statistical analyses

IBM SPSS 20 statistical package was used for analyses. All continuous variable distributions (MRI volumes and symptom inventory scores) were tested for normality with the Shapiro–Wilk test. We used logarithmic transformations to correct for non-normal distribution. In all cases where transformations were utilized, statistical analyses were run on transformed data; however, descriptive data and visual displays depict untransformed data. Chi-square analyses were utilized to test for group differences in the proportion of subjects with neuroradiologic anomalies detected on visual review. General linear modeling was used to test for group differences in total WMH volume, with and without TSBV as a covariate. A WMH-corrected volume was derived by subtracting WMH clusters in the perivascular spaces and gray–white matter junction from the total WMH volume and this WMH-corrected volume was compared between the ASD and TDC groups, with and without TSBV as a covariate. General linear modeling was used to test for group differences in WMH volume and WMH-corrected volume in the secondary, multi-site sample, with and without TSBV entered as a covariate, and with site entered as a fixed factor. Partial correlations between WMH volumes and age and symptom severity were performed in the primary NYU sample, with TSBV as a covariate. The relationship between WMH volume and symptom severity was assessed across three behavioral domains (social, communication,

stereotyped behaviors) and two modalities (clinician-rated and parent-reported).

3. Results

3.1. Sample characteristics

3.1.1. Primary single-scanner sample

There were no differences in age between the ASD and TDC group (Table 1). Handedness was established with the Edinburgh Handedness Inventory (Oldfield, 1971). The ASD group had a greater tendency to left-handedness than the TDC group (Table 1), as well as lower Full-Scale IQ and Verbal IQ, as is commonly observed in ASD samples (Fombonne, 1999; American Psychiatric Association, 2013; Lindell and Hudry, 2013).

3.1.2. Secondary, multi-site sample

Participants from the ASD and the TDC group ranged in age from 8 to 29 years. There were no differences in average age between the ASD and TDC group $t(158) = -0.41$; $p = 0.97$. Categorical information regarding handedness status was available from each site. The proportion of left-handed (N = 10), ambidextrous (N = 2), and right-handed participants (N = 68) in the ASD group did not differ from the proportion of left-handed (N = 3), ambidextrous (N = 3), and right-handed (N = 74) participants in the TDC group ($\chi^2 = 4.2$; $p = 0.12$). Full-Scale IQ data was also available from each site (Table 2). Similar to the primary

Table 3
Results from conventional visual analysis of MRI scans.

Neuroradiologic anomalies	ASD	TDC
Ventriculomegaly	7	5
Transmantle sign	1	0
Dysmorphic posterior corpus callosum	1	0
Hippocampal atrophy	1	0
Abnormal hippocampal shape	3	1
Periventricular heterotopia	1	1
Posterior atrophy	1	1
Arachnoid cyst	0	1
Total	15	9

Normal variant findings	ASD	TDC
Ventricular asymmetry	6	6
Perivascular spaces (i.e., Virchow–Robins Spaces)	17	12
Enlarged temporal horn	1	1
Mammillary body hypoplasia	0	2
Cavum septum vergae	0	2
Total	24	23

ASD = autism spectrum disorder; TDC = typically developing control.

sample, average Full-Scale IQ was lower in the ASD group relative to the TDC group [$t(156) = -3.07$; $p = 0.003$]. Table 2 provides site-specific descriptive information.

3.2. Visual review of research dedicated MRI scans

Blinded visual review revealed no difference in the proportion of individuals with imaging anomalies between the ASD and TDC groups: $\chi^2 = 2.12$; $p = 0.15$. In addition, there was no difference in the proportion of individuals with normal variant findings between the ASD and TDC groups: $\chi^2 = 0.04$; $p = 0.84$. Detailed results from visual review are provided in Table 3. Some individuals may have had more than one neuroradiologic and/or normal variant finding. The number of actual findings for each group is reported in Table 3; whereas, the proportion of ASD and TDC individuals with one or more findings was statistically compared. Given that enlarged perivascular spaces (i.e., Virchow–Robins Spaces) have been previously associated with ASD (Taber et al., 2004), we performed an additional analysis of group differences in the proportion of individuals with enlarged perivascular spaces; however, there was no difference between the ASD and TDC group: $\chi^2 = 1.24$; $p = 0.27$.

3.3. Group comparison of total WMH volume: primary single-scanner sample

Total WMH volumes in the combined ASD and TDC sample were not normally distributed due to the presence of several positive outliers [$W(96) = 0.94$; $p = 0.0002$]; therefore, a logarithmic transformation was applied, resulting in a normal distribution [$W(96) = 0.99$; $p = 0.9$]. Total WMH volumes were elevated in the ASD relative to the TDC group [$t(94) = 2.57$; $p = 0.01$]. The average untransformed total WMH volume in the ASD group was 2068.63 mm^3 (SD = 655.48 mm^3), which was greater than the average total WMH volume of 1765.33 mm^3 (SD = 619.99 mm^3) in the TDC group (see Table 4).

Group differences in TSBV were also tested, as was the correlation between total WMH volume and TSBV. TSBV was normally distributed [$W(96) = 0.99$; $p = 0.9$]. There were no group differences in TSBV [$t(94) = 0.76$; $p = 0.19$]; however, there was a positive correlation between TSBV and total WMH volume in the combined ASD and TDC group [$r = 0.5$; $p = 0.0000001$]. This positive correlation was present in the TDC group alone [$r = 0.62$; $p = 0.000003$] and the ASD group alone [$r = 0.49$; $p = 0.0004$]. Group differences in total WMH volume were still present when TSBV was entered as a covariate [$F = 15.22$; $p = 0.0002$].

3.4. Subregional WMH volumes: primary single-scanner sample

WMH clusters were found in perivascular spaces (Fig. 2A), deep subcortical white matter, periventricular regions (Fig. 2B–C), and superficial white matter regions adjacent to the gray–white matter junction. In the ASD group, 15% of the total WMH volume was accounted for by labeling of the perivascular spaces, which were manually removed

before calculating remaining subregional volumes. The largest portion of the remaining WMH volumes (70%) were in the periventricular region (left lateral ventricle: 43%; left inferior ventricle: 0.5%; right lateral ventricle: 26%; right inferior ventricle: <0.1%). The next largest portion (19%) was in the deep subcortical white matter and the smallest portion (11%) in the gray–white matter junction. A similar pattern was observed in the TDC group: 7% of the total WMH volume was accounted for by labeling of the perivascular spaces. After the removal of these clusters, 74% of the remaining clusters were from the periventricular region (left lateral ventricle: 46%; left inferior ventricle: <0.5%; right lateral ventricle: 28%; right inferior ventricle: <0.1%). The remaining WMH clusters were in the deep subcortical white matter (15%) and gray–white matter junction (11%). Groupwise descriptive information and between-group effect sizes for total and subregional WMH volumes are provided in Table 4.

Visual inspection of clusters in the gray–white matter boundary region revealed that several may have resulted from partial volume effects, in which the intensity of the white matter is contaminated by local cortical gray matter (Shafee et al., 2015); therefore, WMH clusters from the gray–white matter junction were excluded from the total WMH volumes. Subtraction of WMH-labeled clusters in the perivascular spaces and gray–white matter junction resulted in a "WMH-corrected" volume that included only WMH clusters from the periventricular and deep subcortical regions. Group differences in WMH-corrected volume were significantly elevated in ASD [$F = 4.69$; $p = 0.03$], and remained elevated after entering TSBV as a covariate [$F = 9.63$; $p = 0.0002$].

3.5. WMH volume and WMH-corrected volume: independent, multi-site sample

Similar to the primary single-site sample, there were several positive WMH volume outliers in the multi-site sample resulting in a non-normal distribution; therefore, logarithmic transformation was applied to the total WMH volume measure. Total WMH volume was elevated in the ASD group relative to the TDC group [$F = 12.92$; $p = 0.0004$; ASD: mean = 2367.7 mm^3 (SD = 1271.74 mm^3); TDC: mean = 1883.74 mm^3 (SD = 742.13 mm^3)] (Fig. 3). There was also a main effect of site on total WMH volume ($F = 4.77$; $p = 0.00008$) but no interaction between group and site ($F = 1.13$; $p = 0.0035$).

There were no group differences in TSBV [$t(158) = 0.62$; $p = 0.53$]; however, there was a positive correlation between TSBV and total WMH volume in the combined ASD and TDC group [$r = 0.19$; $p = 0.02$]. Group differences in total WMH volume remained significant after controlling for TSBV [$F = 11.15$; $p = 0.001$], which replicates findings obtained in the primary NYU sample. In addition, there were group differences in WMH-corrected volumes [$F = 12.36$; $p = 0.001$], which remained significant after controlling for TSBV [$F = 10.77$; $p = 0.001$]. There was a main effect of site on WMH-corrected volumes [$F = 7.08$; $p = 0.0001$] but no interaction between group and site [$F = 1.06$; $p = 0.39$]. This demonstrates that elevated periventricular/deep subcortical WMH volumes in ASD were replicated across two independent samples and were independent of variation attributable to site differences. Groupwise

Table 4
Group differences in total and subregional WMH volumes in the primary NYU sample.

	ASD mean (SD)	TDC mean (SD)	F-value[*]	p-value
Total WMHV (mm^3)	2068.63 (655.48)	1765.33 (619.99)	15.22	0.0002[**]
Periventricular WMHV (mm^3)	1441.21 (411.08)	1308.71 (423.99)	8.84	0.004[**]
Subcortical WMHV (mm^3)	346.06 (396.35)	249.93 (289.1)	4.12	0.045[*]
GWJ WMHV (mm^3)	229.6 (150.12)	188.04 (143.76)	5.02	0.027[*]
Perivascular WMHV (mm^3)	51.76 (167.6)	18.65 (54.65)	1.94	0.17
WMHV-corrected (mm^3) [Total − (GWJ + PVS)]	1787.26 (586.58)	1558.64 (540.11)	9.63	0.003[**]

ASD = Autism Spectrum Disorder; TDC = Typically Developing Control; WMHV = white matter hypointensity volume; GWJ = cortical gray–white junction; PVS = perivascular spaces.
 [*] Sig at $p < 0.05$ with total brain volume as a covariate.
  [**] Sig at $p < 0.005$ with total brain volume as a covariate.
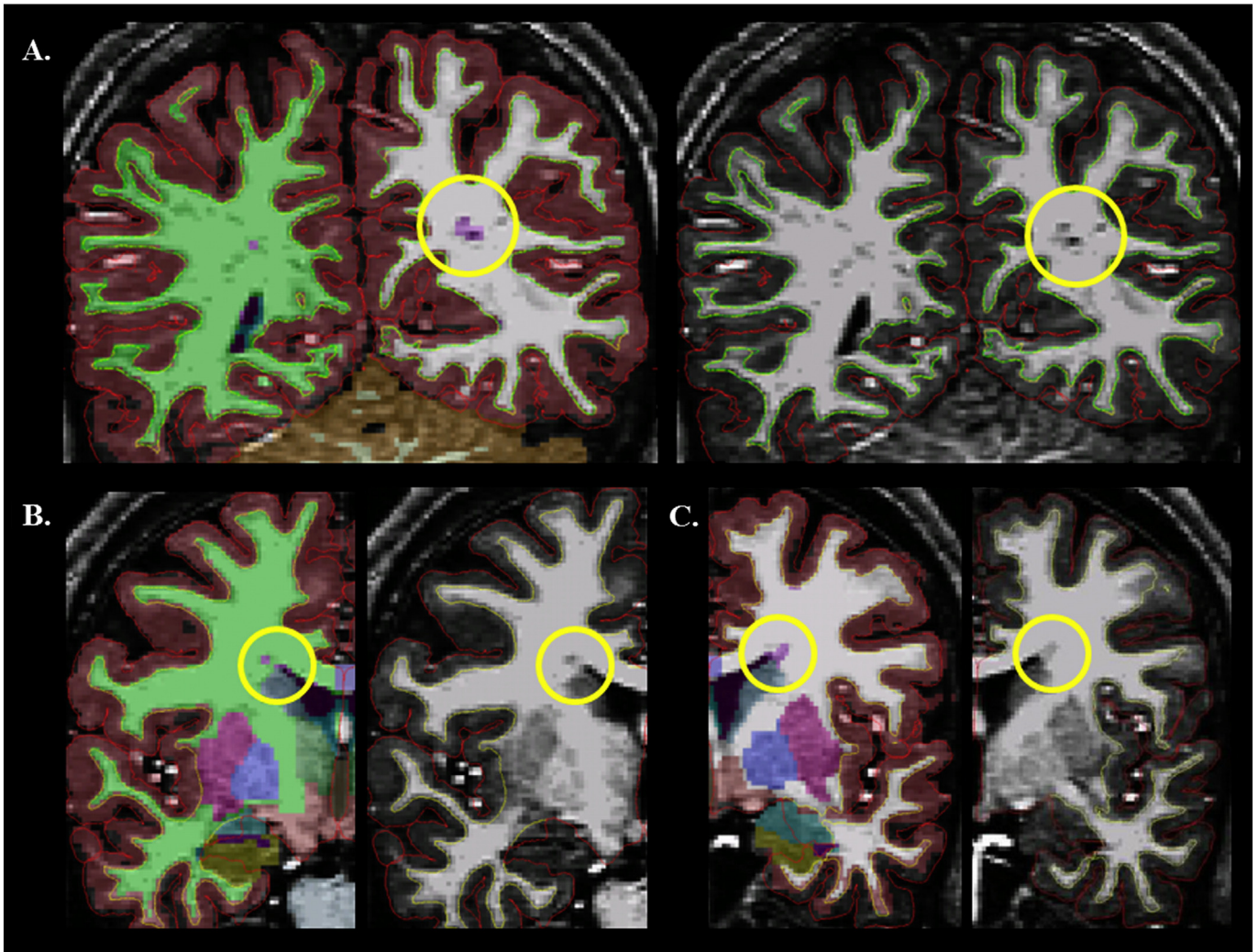
Fig. 2. Location of WMH-labeled clusters. Images depict T1-weighted scans of individual ASD participants. The subcortical segmentation overlay is depicted on the left-sided images for A–C. WMH clusters are purple (circled). (A) WMH cluster in the perivascular region; (B–C) WMH clusters in the periventricular region.

descriptive information and between-group effect sizes for total and subregional WMH volumes in the secondary, multi-site sample are provided in Table 5.
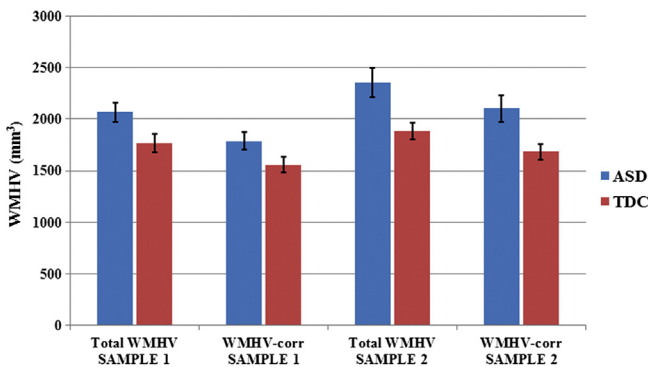
Fig. 3. White matter hypointensity volumes (WMHV) are elevated in ASD. Bar graph depicting group differences in total average WMHV and WMHV-corrected (WMHV-corr) volumes. WMHV-corr volumes include only the periventricular and deep subcortical white matter clusters. Blue bars depict the autism spectrum disorder (ASD) group and red bars depict the typically developing control (TDC) group. Sample 1 refers to the primary single-scanner NYU sample (48 ASD/48 TDC). Sample 2 refers to the secondary multi-site sample (80 ASD/80 TDC). Error bars depict standard error.

3.6. Do periventricular/deep subcortical WMH change with age?

There was no correlation between the age of participants and (log-transformed) WMH-corrected volumes for the combined ASD and TDC group ($r = -0.14$; $p = 0.17$), the TDC group alone ($r = -0.10$; $p = 0.50$), or the ASD group alone ($r = -0.18$; $p = 0.22$). WMH-corrected volume was positively associated with TSBV ($r = 0.42$; $p = 0.00002$) and TSBV was negatively correlated with age ($r = -0.23$; $p = 0.03$); therefore, we performed a partial correlation between WMH-corrected volumes and age, controlling for TSBV; results were also not significant for the whole group ($r = -0.05$; $p = 0.61$), the TDC group ($r = -0.11$; $p = 0.45$), or the ASD group ($r = -0.06$; $p = 0.71$). These findings indicate that periventricular/deep subcortical WMH volume does not change with age in children/young adults.

3.7. Are periventricular/deep subcortical WMH associated with symptom severity?

There was no correlation between WMH-corrected volume and ADOS-G total algorithm scores ($r = 0.12$; $p = 0.46$). Within the specific ADOS-G subscales, WMH-corrected volume was positively correlated with the SBRI subscale ($r = 0.36$; $p = 0.02$) (Fig. 4A) but not the SI ($r = 0.02$; $p = 0.89$) or Comm ($r = 0.28$; $p = 0.07$) subscales. A similar pattern was observed with the ADOS revised algorithm scores (Gotham

Table 5
Group differences in total and subregional WMH volumes in the multi-site sample.

	ASD mean (SD)	TDC mean (SD)	F-value	p-value
Total WMHV (mm^3)	2367.7 (1271.74)	1883.74 (742.13)	11.15	0.001**
Periventricular WMHV (mm^3)	1612.53 (633.04)	1391.06 (471.94)	8.32	0.005**
Subcortical WMHV (mm^3)	501.18 (771.18)	294.09 (308.1)	5.69	0.02*
GWJ WMHV (mm^3)	241.48 (271.82)	183.3 (157.55)	2.46	0.12
Perivascular WMHV (mm^3)	12.51 (37.61)	15.29 (48.43)	0.18	0.67
WMHV-corrected (mm^3) [Total − (GWJ + PVS)]	2113.71 (1152.09)	1685 (659.33)	10.77	0.001**

ASD = Autism Spectrum Disorder; TDC = Typically Developing Control; WMHV = white matter hypointensity volume; GWJ = cortical gray–white junction; PVS = perivascular spaces.
  * Sig at p < 0.05 with site as a fixed factor and total supratentorial brain volume as a covariate.
  ** Sig at p < 0.001 with site as a fixed factor and total supratentorial brain volume as a covariate.

et al., 2007); there was a positive correlation between WMH-corrected volume and Gotham-RRB scores ($r = 0.42$; $p = 0.01$), but not the Gotham-SA ($r = 0.05$; $p = 0.77$) or Gotham-Sev ($r = 0.14$; $p = 0.44$) scores. Within the ADI-R indices, WMH-corrected volume was positively correlated with the RRB index ($r = 0.31$; $p = 0.05$) (Fig. 4B). Correlations between WMH-corrected and the social ($r = 0.29$; $p = 0.07$) and verbal ($r = 0.3$; $p = 0.06$) indices were similar in effect size but were not significant. Taken together, these results suggest a consistent relationship between periventricular/deep subcortical WMH volume and restricted repetitive behaviors across different measurement modalities (clinician-rated and parent-reported).

4. Discussion

This study implicates periventricular white matter abnormalities in the presentation of ASD, particularly in restricted repetitive behaviors, one of the core diagnostic features. Using a quantitative approach, we found an ASD-associated elevation in WMH volume across two independent samples. WMH volume elevations in ASD were robust to site-related variance in the secondary multi-site sample. The majority of WMH clusters were located in the periventricular region, with smaller proportions also found in the deep subcortical white matter, cortical gray–white matter junction, and perivascular spaces. Elevated periventricular and deep subcortical WMH volume in the ASD group was associated with a higher degree of restricted repetitive behaviors on both ADOS and ADI-R indices; thus demonstrating consistent findings across clinician-rated and parent-reported symptom inventories.

Given the robustness of ASD associated elevations in periventricular and deep subcortical WMH across independent samples, as well as a consistent relationship with restricted repetitive behaviors across different symptom measurement modalities, our results raise important questions about the nature of elevated WMH in ASD and its relationship

to behavioral stereotypies. What might be the histological basis for focal WMH clusters? Does the relationship between elevated periventricular WMH volumes and restricted repetitive behaviors reflect disruption of frontal–subcortical networks subserving behavioral monitoring and control? Could morphometric MRI analysis offer unique diagnostic information in a comprehensive workup for children and young adults with ASD?

4.1. What is the potential etiology of T1-weighted white matter hypointensities?

Delayed white matter development is a common MRI finding in ASD (Cheng et al., 2010; Lee et al., 2007; Shukla et al., 2011; Wolff et al., 2012). In infants at high risk for ASD, abnormalities in fractional anisotropy (FA) are apparent as early as 6 months with blunted growth trajectories evident by 12 months (Wolff et al., 2012). In adolescents and adults, the age-related FA increases and mean diffusivity (MD) decreases that are apparent in normative samples across several long-range tracts, are diminished in ASD (Cheng et al., 2010; Lee et al., 2007; Shukla et al., 2011). This raises the possibility that WMH volume provides an alternative measure of delayed or blunted white matter development. Regions of reduced myelination might appear as hypointense on T1-weighted images and increased volume of T1-weighted hypointense clusters could reflect blunted myelination trajectories in ASD. However, the absence of age effects on WMH volume in the TDC group, the ASD group, and the combined TDC and ASD groups does not support this interpretation. This is not to suggest that WMH is independent from myelination. Myelination failures could lead to WMH clusters; however, the absence of age effects indicates that these focal abnormalities in signal intensity reflect static anomalies rather than maturational delays.
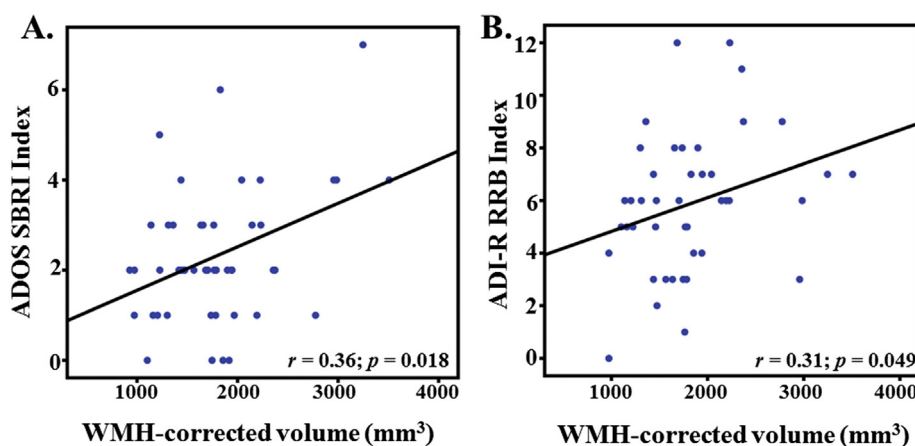
Fig. 4. Scatterplots depicting linear relationship between WMH-corrected volumes (i.e., periventricular and deep subcortical WMH volume) and A.) Autism Diagnostic Observation Schedule Stereotyped Behaviors and Repetitive Interests; and B.) Autism Diagnostic Inventory–Revised Restrictive, Repetitive Behaviors.

Factors leading to static morphometric anomalies could include early environmental perturbations (e.g., maternal infection, inflammation, prenatal brain injury) and/or genetic mutations. Rodent offspring exposed to streptococcal maternal infection show autistic symptoms and patches of periventricular white matter loss (Bergeron et al., 2013). Similarly, in preterm newborns, positive results on an autism screening tool at 2-year follow-up are associated with a history of chorioamnionitis (by placental pathology), as well as periventricular white matter damage on MRI (Limperopoulos et al., 2008).

The role of genetic factors remains uncertain in our sample; whole genome microarrays, extensive ASD panels, and whole exome sequencing were not performed. Therefore, some participants likely carried deleterious mutations associated with high risk of ASD (Pinto et al., 2010). Such mutations could result in a range of brain anomalies that at the positive extreme could lead to exclusion from the study but to a lesser degree only be revealed by quantitative comparison to controls (Stefansson et al., 2014). For example, mutations of the PTEN tumor suppressor gene are associated with aberrant brain growth (i.e., macrocephaly) and ASD symptoms (Butler et al, 2005; Lynch et al., 2009; Varga et al., 2009); however, neuroradiologic findings are variable with normal findings in some patients and cortical malformations in others (DeLone et al., 1999; Lok et al, 2005; Tan et al., 2007). In a sample of patients with PTEN mutations, quantitatively determined macrocephaly, and developmental delay, all had multifocal periventricular white matter abnormalities, characterized by periventricular hypointense clusters on T1-weighted images (Vanderver et al., 2014). This suggests that similar pathogenic factors might contribute to larger brain volumes and periventricular WMH.

Among a core set of 197 high-risk autism-associated genes (Casanova and Casanova, 2014), 88% show a relationship between the gene product function and neuroblast development. In addition, 80% of the core genes influence post-migratory processes of neuritogenesis, synaptogenesis, and plasticity, primarily by loss-of-function. This indicates that dysfunction within any of the core gene sites can disrupt various processes subserving cortical development, resulting in a variety of malformations. Such morphological abnormalities are found at high rates in postmortem autism studies, with the most common finding being patchy cortical dysplasias in the frontal and temporal lobe (Casanova et al., 2013; Stoner et al., 2014; Wegiel et al., 2010). Subcortical and periventricular heterotopia are less common yet still present at higher rates in ASD than controls (Wegiel et al., 2010). Although elevated periventricular/deep subcortical WMH volumes might reflect increased heterotopic neuronal clusters in ASD, direct correspondence between MRI and histological findings is needed for confirmation.

4.2. Periventricular white matter hypointensities and aberrant striatal–prefrontal networks

Animal models of restricted repetitive behaviors implicate three primary fronto-striatal "loops" supported by periventricular white matter proximal to the striatum (Langen et al., 2011a,b; Lewis and Kim, 2009): striatum-motor, striatum-prefrontal, and striatum-orbitofrontal/cingulate. Disruption of striatum-motor loops can lead to repetitive non-goal-oriented activity such as motor stereotypies (Lewis et al., 2007; Saka et al., 2004). Dysfunction in striatum–prefrontal loops can lead to repetitive goal-oriented behavior such as in obsessive–compulsive behaviors and perseverative thoughts/behaviors (Birrell and Brown, 2000; Dias et al., 1996). Finally, striatum-orbitofrontal/anterior cingulate loops subserve motivational aspects of behavioral control (i.e., reward-seeking behaviors) and when dysfunctional, can lead to impulsive or compulsive behavior (Cardinal et al., 2001; Wyvell and Berridge, 2000). Aberrant connectivity within or between these fronto-striatal loops can result in abnormally expressed restricted repetitive behaviors and interests (Langen et al., 2011a,b).

In humans with ASD, abnormalities of striatal structure, function, and connectivity are commonly observed. Caudate enlargement in ASD is a consistently replicated finding (Haznedar et al., 2006; Hollander

et al., 2005; Langen et al., 2007; Rojas et al., 2006; Sears et al., 1999; Voelbel et al., 2006). Glucose metabolism in the caudate is decreased in ASD, linking volumetric enlargement to decreased function (Haznedar et al, 2006). Furthermore, caudate enlargement in ASD is directly associated with increased restricted repetitive behaviors (Hollander et al., 2005; Langen et al., 2007; Rojas et al., 2006; Sears et al., 1999) and increased impulsivity (Voelbel et al., 2006). Regional glucose metabolism in the caudate and frontal cortical regions is positively correlated in healthy controls but negatively correlated or uncorrelated in adult men with autism (Horwitz et al., 1988). Adults with ASD show reduced FA and increased MD in frontal-striatal tracts (Langen et al., 2012). Resting state functional MRI connectivity between the caudate and premotor/pericentral regions is more diffusely organized in adults with ASD relative to controls (Turner et al., 2006). Diffusely organized striatum-cortical connectivity in ASD extends to the insula, superior temporal, supramarginal, and fusiform regions, all of which are either uncorrelated with the striatum in controls or correlated in the opposite direction (Di Martino et al., 2011). In the absence of age effects, these diffusely organized striatum-cortical networks in ASD have been described as *ectopic*, rather than *residual* (i.e., immature) (Di Martino et al., 2011). Thus, it is possible that periventricular WMH contributes to dysfunctional fronto-striatal networks by disrupting normal connectivity patterns, prompting the formation of more diffusely organized or ectopic fronto-striatal networks.

4.3. Can quantitative MRI findings inform the debate on the diagnostic utility of MRI in ASD?

Visual review of MRI scans has not consistently identified a higher prevalence of imaging findings in children with non-syndromic ASD compared to typically developing controls, despite using comprehensive imaging protocols (Boddaert et al., 2009; Vasa et al., 2012). However, variation in findings might be associated with characteristics of the ASD sample. When the study sample is limited to individuals with high functioning ASD, imaging findings are equivalent between ASD and controls (Vasa et al., 2012). However, when ASD study samples include individuals with lower cognitive levels, higher rates of MRI abnormalities are obtained, including white matter signal abnormalities, dilated Virchow–Robins spaces, T2-weighted white matter hyperintensities and a loss of gray–white matter definition in the temporal poles (Boddaert et al., 2009).

Given this variability in findings, the utility of MRI in the comprehensive workup for ASD is debated. According to the American Academy of Neurology and Child Neurology Society (Filipek et al., 2000), the American Academy of Child and Adolescent Psychiatry (Volkmar et al., 1999), and the American Academy of Pediatrics (Johnson et al., 2007), MRI is not indicated as part of the routine evaluation of children with ASD. Early detection of developmental anomalies could inform treatment decisions such as referral for a more comprehensive electroencephalographic evaluation; yet, the costs of MRI indicate that more robust data is needed to support the diagnostic or prognostic utility of MRI in ASD. This includes discovery of specific MRI findings that are more prevalent in ASD and an association between clinical or etiopathologic aspects of the disorder.

In our study, which included individuals in the borderline to superior (76–142) IQ range, with a mean IQ in the average range (109), we did not find elevated MRI abnormalities on blinded visual analysis. It is important to note that visual review included T1-weighted scans only, which were collected for research purposes. Review of T1-weighted images alone is not sufficient for clinical purposes and was used here only to determine whether gross morphological anomalies were present. Thus, our data cannot address the question of whether subtle malformations of cortical development might be more readily visible on other imaging sequences. However, we did find that the use of quantitative methods allowed for detection of subtle morphological differences between a relatively high functioning group of ASD individuals and TDCs. These findings contribute to the debate on the diagnostic utility of MRI in ASD populations in that they provide evidence of elevated

focal white matter abnormalities in a relatively high-functioning ASD group when quantitative, but not qualitative, analyses were employed. The relationship to restricted repetitive behaviors suggests that elevated periventricular WMH volume is not an incidental finding but is associated with one of the central features of the ASD behavioral phenotype.

4.4. Limitations

In the current dataset, T1-weighted images were the only structural scans available for analysis. A comprehensive imaging protocol including T2-weighted and FLAIR images would be optimal for detection of focal white matter abnormalities. Although this makes the etiology of WMH clusters difficult to infer, interpretation of abnormal signal on T2-weighted images is also limited. Ultimately, only histological data co-registered to the MR images can address this issue. The limitations of relying on a T1-weighted scan are offset by several strengths inherent to the ABIDE sample such as a large number of scans available for analysis, high-resolution anatomical images, uniformity of scanner and sequences, and well-characterized samples.

Enlarged perivascular spaces (i.e., Virchow Robin spaces) in ASD have been previously reported (Taber et al., 2004). However, we did not find a significant group difference in the presence of Virchow Robin spaces using conventional visual analysis. This does not necessarily contradict enlarged perivascular spaces as a relevant finding in ASD. In Taber et al., 2004, grading scales (Heier et al., 1989) were used to rate dilation from smallest (grade 1) to most dilated (grade 3), which resulted in children/adolescents with ASD showing higher rates of grades 2 and 3 perivascular spaces than controls. We did not utilize a similar grading scale in our visual analysis. Although WMH labeling of perivascular spaces provides an alternative to a visual grading system, examination of WMH segmentation and labeling outcomes revealed that enlarged perivascular spaces, as diagnosed by visual review, were not consistently labeled as WMH in the automated segmentation routine. Out of the 29 individuals noted to have enlarged perivascular spaces on CVA, 26 were labeled WMH and three were not labeled WMH (conversely, two were labeled WMH but missed on CVA). In addition, the full extent of the perivascular spaces was not always labeled. For example, grading systems (Heier et al., 1989) upgrade ratings to the next level if there are several small proximal spaces; however, WMH labeling did not consistently label each of these spaces when present. This suggests that perivascular WMH volume likely underestimates the volume of perivascular spaces and should be interpreted with reserve.

An additional limitation is that diagnosis was based on DSM-IV-TR; therefore, results may be less generalizable to individuals with a DSM-5 based Autism Spectrum Disorder diagnosis. Given the removal of verbal deficits as a core diagnostic feature of ASD in DSM-5 criteria, samples derived from the DSM-5 may be comprised of higher functioning individuals. However, when combined ADOS/ADI-R data is used to establish an ASD diagnosis, the majority of participants (93%) meet DSM-5 criteria for ASD (Mazefsky et al., 2013). Furthermore, in our sample, elevated WMH volume was associated with stereotyped behaviors and restricted interests, a domain that remains a core diagnostic feature of ASD in the DSM-5.

Finally, the current sample excluded individuals with a history of intellectual disability (ID) or epilepsy; therefore, our results are generalizable only to the subset of individuals with ASD without these comorbidities. Future studies should make an effort to include individuals with comorbid epilepsy and/or ID to determine if elevated WMH volume is related to seizure severity or deficits in intellectual functioning.

Disclosures

All authors report no biomedical financial interests or potential conflicts of interest.

Appendix A

Table A.1
Multi-site sample scanner and sequence parameters.

Site	Scanner	Sequence parameters
PITT	Siemens 3 T Allegra	TE = 3.93 ms, TR = 2100 ms, TI = 1000 ms, flip angle = 7°, FOV = 269 mm, voxel size = 1.1 × 1.1 × 1.1 mm
OHSU	Siemens 3 T Tim Trio	TE = 3.58 ms, TR = 2300 ms, TI = 900 ms, flip angle = 10°, FOV = 256 mm, voxel size = 1 × 1 × 1.1 mm
SDSU	GE 3 T MR750	TE = 4.3, TR = 2300 ms, TI = 600 ms, flip angle = 45°, FOV = 256 mm, voxel size = 1.3 × 1.3 × 1.3 mm
USM	Siemens 3 T Tim Trio	TE = 2.91, TR = 2300 ms, TI = 900 ms, flip angle = 9°, FOV = 256 mm, voxel size = 1 × 1 × 1.2 mm
CMU	Siemens 3 T Verio	TE = 2.48, TR = 1870 ms, TI = 1100 ms, flip angle = 8°, FOV = 256 mm, voxel size = 1 × 1 × 1 mm
KKI	3 T Philips Achieva	TE = shortest, TR = shortest; flip angle = 8°, voxel size = 1 × 1 × 1 mm
UCLA	Siemens 3 T Tim Trio	TE = 2.84, TR = 2300 ms, TI = 853 ms, flip angle = 9°, FOV = 256 mm, voxel size = 1 × 1 × 1.2 mm
CALTECH	Siemens 3 T Tim Trio	TE = 2.73, TR = 1590 ms, TI = 800 ms, flip angle = 10°, FOV = 256 mm, voxel size = 1 × 1 × 1 mm

PITT = University of Pittsburgh School of Medicine; OHSU = Oregon Health and Science University; SDSU = San Diego State University; USM = Utah School of Medicine; CMU = Carnegie Melon University; KKI = Kennedy Krieger Institute; UCLA = University of California Los Angeles; CALTECH = California Institute of Technology; 3 T = 3-Tesla; TE = echo time; TR = relaxation time; FOV = field of view.

References

American Psychiatric Association, 2013. Diagnostic and Statistical Manual of Mental Disorders. 5th ed. American Psychiatric Publishing, Arlington, VA.

Bergeron, J.D., Deslauriers, J., Grignon, S., Fortier, L.C., Lepage, M., Stroh, T., et al., 2013. White matter injury and autistic-like behavior predominantly affecting male rat offspring exposed to group B streptococcal maternal inflammation. Dev. Neurosci. 35, 504–515.

Bernasconi, A., Bernasconi, N., Bernhardt, B.C., Schrader, D., 2011. Advances in MRI for 'cryptogenic' epilepsies. Nat. Rev. Neurol. 7, 99–108.

Birrell, J.M., Brown, V.J., 2000. Medial frontal cortex mediates perceptual attentional set shifting in the rat. J. Neurosci. 20, 4320–4324.

Boddaert, N., Zilbovicius, M., Philipe, A., Robel, L., Bourgeois, M., Barthelemy, C., et al., 2009. MRI findings in 77 children with non-syndromic autistic disorder. PLoS ONE 4, e4415.

Butler, M.G., Dasouki, M.J., Zhou, X.P., Talebizadeh, Z., Brown, M., Takahashi, T.N., et al., 2005. Subset of individuals with autism spectrum disorders and extreme macrocephaly associated with germline PTEN tumour suppressor gene mutations. J. Med. Genet. 42, 318–321.

Cardinal, R.N., Pennicott, D.R., Sugathapala, C.L., Robbins, T.W., Everitt, B.J., 2001. Impulsive choice induced in rats by lesions of the nucleus accumbens core. Science 292, 2499–2501.

Casanova, E.L., Casanova, M.F., 2014. Genetics studies indicate that neural induction and early neuronal maturation are disturbed in autism. Front. Cell. Neurosci. 8, 397.

Casanova, M.F., El-Baz, A.S., Kamat, S.S., Dombroski, B.A., Khalifa, F., Elnakib, A., et al., 2013. Focal cortical dysplasias in autism spectrum disorders. Acta Neuropathol. Commun. 1, 67.

Cheng, Y., Chou, K.H., Chen, I.Y., Fan, Y.T., Decety, J., Lin, C.P., 2010. Atypical development of white matter microstructure in adolescents with autism spectrum disorders. Neuroimage 50, 873–882.

Colombo, N., Salamon, N., Raybaud, C., Ozkara, C., Barkovich, A.J., 2009. Imaging of malformations of cortical development. Epileptic Disord. 11, 194–205.

DeLone, D.R., Brown, W.D., Gentry, L.R., 1999. Proteus syndrome: craniofacial and cerebral MRI. Neuroradiology 41, 840–843.

Di Martino, A., Kelly, C., Grzadzinski, R., Zuo, X.N., Mennes, M., Mairena, M.A., et al., 2011. Aberrant striatal functional connectivity in children with autism. Biol. Psychiatry 69, 847–856.

Di Martino, A., Yan, C.G., Li, Q., Denio, E., Castellanos, F.X., Alaetrs, K., et al., 2014. The autism brain imaging data exchange: towards a large-scale evaluation of the intrinsic brain architecture in autism. Mol. Psychiatry 19, 659–667.

Dias, R., Robbins, T.W., Roberts, A.C., 1996. Dissociation in prefrontal cortex of affective and attentional shifts. Nature 380, 69–72.

Ecker, C., Murphy, D., 2014. Neuroimaging in autism—from basic science to translational research. Nat. Rev. Neurol. 10, 82–91.

Filipek, P.A., Accardo, P.J., Ashwal, S., Baranek, G.T., Cook Jr., E.H., Dawson, G., et al., 2000. Practice parameter: screening and diagnosis of autism: report of the Quality Standards Subcommittee of the American Academy of Neurology and the Child Neurology Society. Neurology 55, 468–479.

Fischl, B., Salat, D.H., Busa, E., Albert, M., Dieterich, M., Haselgrove, C., van der Kouwe, A., et al., 2002. Whole brain segmentation: automated labeling of neuroanatomical structures in the human brain. Neuron 33, 341–355.

Fombonne, E., 1999. The epidemiology of autism: a review. Psychol. Med. 29, 769–786.

Gotham, K., Risi, S., Pickles, A., Lord, C., 2007. The Autism Diagnostic Observation Schedule: revised algorithms for improved diagnostic validity. J. Autism Dev. Disord. 37 (4), 613–627.

Happé, F., Ronald, A., Plomin, R., 2006. Time to give up on a single explanation for autism. Nat. Neurosci. 9, 1218–1220.

Haznedar, M.M., Buchsbaum, M.S., Hazlett, E.A., LiCalzi, E.M., Cartwright, C., Hollander, E., 2006. Volumetric analysis and three-dimensional glucose metabolic mapping of the striatum and thalamus in patients with autism spectrum disorders. Am. J. Psychiatry 163, 1252–1263.

Heier, L.A., Bauer, C.J., Schwartz, L., Zimmerman, R.D., Morgello, S., Deck, M.D., 1989. Large Virchow–Robin spaces: MR-clinical correlation. Am. J. Neuroradiol. 10, 929–936.

Hollander, E., Anagnostou, E., Chaplin, W., Esposito, K., Haznedar, M.M., LaCalzi, E., et al., 2005. Striatal volume on magnetic resonance imaging and repetitive behaviors in autism. Biol. Psychiatry 58, 226–232.

Horwitz, B., Rumsey, J.M., Grady, C.L., Rapoport, S.I., 1988. The cerebral metabolic landscape in autism. Intercorrelations of regional glucose utilization. Arch. Neurol. 45, 749–755.

Johnson, C.P., Myers, S.M., American Academy of Pediatrics Council on Children With Disabilities, 2007. Identification and evaluation of children with autism spectrum disorders. Pediatrics 120, 1183–1215.

Jovicich, J., Czanner, S., Greve, D., Haley, E., van de Kouwe, A., Gollub, R., et al., 2006. Reliability in multi-site structural MRI studies: effects of gradient non-linearity correction on phantom and human data. Neuroimage 30, 436–443.

KucharskyHiess, R., Alter RA, Sojoudi S., Ardekani, B., Kuzniecky, R., Pardoe, H.R., 2015. Corpus callosum area and brain volume in autism spectrum disorder: quantitative analysis of structural MRI from the ABIDE database. J. Autism Dev. Disord. http://dx.doi.org/10.1007/s10803-015-2468-8 (Jun 5 epub ahead of print).

Lai, M.C., Lombardo, M.V., Chakrabarti, B., Baron-Cohen, S., 2013. Subgrouping the autism 'spectrum': reflections on DSM-5. PLoS Biol. 11, e1001544.

Langen, M., Durston, S., Staal, W.G., Palmen, S.J., van Engeland, H., 2007. Caudate nucleus is enlarged in high-functioning medication-naive subjects with autism. Biol. Psychiatry 62, 262–266.

Langen, M., Durston, S., Kas, M.J.H., van Engeland, H., Staal, W.G., 2011a. The neurobiology of repetitive behavior: ...and men. Neurosci. Biobehav. Rev. 35, 356–365.

Langen, M., Kas, M.J.H., Staal, W.G., van Engeland, H., Durston, S., 2011b. The neurobiology of repetitive behavior: of mice.... Neurosci. Biobehav. Rev. 35, 345–355.

Langen, M., Leemans, A., Johnston, P., Ecker, C., Daly, E., Murphy, C.M., et al., 2012. Frontostriatal circuitry and inhibitory control in autism: findings from diffusion tensor imaging tractography. Cortex 48, 183–193.

Lee, J.E., Bigler, E.D., Alexander, A.L., Lazar, M., DuBray, M.B., Chung, M.K., et al., 2007. Diffusion tensor imaging of white matter in the superior temporal gyrus and temporal stem in autism. Neurosci. Lett. 424, 127–132.

Lewis, M., Kim, S.J., 2009. The pathophysiology of restricted repetitive behavior. J. Neurodev. Disord. 1, 114–132.

Lewis, M.H., Tanimura, Y., Lee, L.W., Bodfish, J.W., 2007. Animal models of restricted repetitive behavior in autism. Behav. Brain Res. 176, 66–74.

Limperopoulos, C., Bassan, H., Sullivan, N.R., Soul, J.S., Robertson, R.L., Moore, M., et al., 2008. Positive screening for autism in ex-preterm infants: prevalence and risk factors. Pediatrics 121, 758–765.

Lindell, A.K., Hudry, K., 2013. Atypicalities in cortical structure, handedness, and functional lateralization for language in autism spectrum disorders. Neuropsychol. Rev. 23 (3), 257–270.

Lok, C., Viseux, V., Avril, M.F., Richard, M.A., Gondry-Jouet, C., Deramond, H., et al., 2005. Brain magnetic resonance imaging in patients with Cowden syndrome. Medicine (Baltimore) 84, 129–136.

Lord, C., Rutter, M., Le Couteur, A., 1994. Autism Diagnostic Interview—Revised: a revised version of a diagnostic interview for caregivers of individuals with possible pervasive developmental disorders. J. Autism Dev. Disord. 24, 659–685.

Lord, C., Risi, S., Lambrecht, L., Cook Jr., E.H., Leventhal, B.L., DiLavore, P.C., Pickles, A., Rutter, M., 2000. The autism diagnostic observation schedule-generic: a standard measure of social and communication deficits associated with the spectrum of autism. J. Autism Dev. Disord. 30 (3), 205–223.

Lynch, N.E., Lynch, S.A., McMenamin, J., Webb, D., 2009. Bannayan–Riley–Ruvalcaba syndrome: a cause of extreme macrocephaly and neurodevelopmental delay. Arch. Dis. Child. 94, 553–554.

Mazefsky, C.A., McPartland, J.C., Gastgeb, H.Z., Minshew, N.J., 2013. Brief report: comparability of DSM-IV and DSM-5 ASD research samples. J. Autism Dev. Disord. 43, 1236–1242.

Oldfield, R.C., 1971. The assessment and analysis of handedness: the Edinburgh inventory. Neuropsychologia 9 (1), 97–113.

Pardoe, H.R., Mandelstam, S.A., Hiess, R.K., Kuzniecky, R.I., Jackson, G.D., Alzheimers Disease Neuroimaging Initiative, Epilepsy Phenome/Genome Project Investigators, 2015. Quantitative assessment of corpus callosum morphology in periventricular nodular heterotopia. Epilepsy Res. 109, 40–47.

Pascher, B., Kröll, J., Mothersill, I., Krämer, G., Huppertz, H.J., 2013. Automated morphometric magnetic resonance imaging analysis for the detection of periventricular nodular heterotopia. Epilepsia 54, 305–313.

Pinto, D., Pagnamenta, A.T., Klei, L., Anney, R., Merico, D., Regan, R., et al., 2010. Functional impact of global rare copy number variation in autism spectrum disorders. Nature 466 (7304), 368–372.

Reuter, M., Tisdall, M.D., Qureshi, A., Buckner, R.L., van der Kouwe, A.J., Fischl, B., et al., 2015. Head motion during MRI acquisition reduces gray matter volume and thickness estimates. Neuroimage 107, 107–115.

Rojas, D.C., Peterson, E., Winterrowd, E., Reite, M.L., Rogers, S.J., Tregellas, J.R., 2006. Regional gray matter volumetric changes in autism associated with social and repetitive behavior symptoms. BMC Psychiatry 6, 56.

Saka, E., Goodrich, C., Harlan, P., Madras, B.K., Graybiel, A.M., 2004. Repetitive behaviors in monkeys are linked to specific striatal activation patterns. J. Neurosci. 24, 7557–7565.

Sears, L.L., Vest, C., Mohamed, S., Bailey, J., Ranson, B.J., Piven, J., 1999. An MRI study of the basal ganglia in autism. Prog. Neuro-Psychopharmacol. Biol. Psychiatry 23, 613–624.

Shafee, R., Buckner, R.L., Fischl, B., 2015. Gray matter myelination of 1555 human brains using partial volume corrected MRI image. Neuroimage 105, 473–485.

Shukla, D.K., Keehn, B., Müller, R.A., 2011. Tract-specific analyses of diffusion tensor imaging show widespread white matter compromise in autism spectrum disorder. J. Child Psychol. Psychiatry 52, 286–295.

Sled, J.G., Zijdenbos, A.P., Evans, A.C., 1998. A nonparametric method for automatic correction of intensity nonuniformity in MRI data. IEEE Trans. Med. Imaging 17, 87–97.

Stefansson, H., Meyer-Lindenberg, A., Steinberg, S., Magnusdottir, B., Morgen, K., Arnarsdottir, et al., 2014. CNVs conferring risk of autism or schizophrenia affect cognition in controls. Nature 505, 361–366.

Stoner, R., Chow, M.L., Boyle, M.P., Sunkin, S., Mouton, P.R., Roy, S., et al., 2014. Patches of disorganization in the neocortex of children with autism. N. Engl. J. Med. 370, 1209–1219.

Taber, K.H., Shaw, J.B., Loveland, K.A., Pearson, D.A., Lane, D.M., Hayman, L.A., et al., 2004. Accentuated Virchow–Robin spaces in the centrum semiovale in children with autistic disorder. J. Comput. Assist. Tomogr. 28, 263–268.

Tan, W.H., Baris, H.N., Burrows, P.E., Robson, C.D., Alomari, A.I., Mulliken, J.B., et al., 2007. The spectrum of vascular anomalies in patients with PTEN mutations: implications for diagnosis and management. J. Med. Genet. 44, 594–602.

Tuchman, R., Moshé, S.L., Rapin, I., 2009. Convulsing toward the pathophysiology of autism. Brain Dev. 31, 41.

Turner, K.C., Frost, L., Linsenbardt, D., McIlroy, J.R., Müller, R.A., 2006. Atypically diffuse functional connectivity between caudate nuclei and cerebral cortex in autism. Behav. Brain Funct. 2, 34.

Vanderver, A., Tonduti, D., Kahn, I., Schmidt, J., Medne, L., Vento, J., et al., 2014. Characteristic brain magnetic resonance imaging pattern in patients with macrocephaly and PTEN mutations. Am. J. Med. Genet. A164A, 627–633.

Varga, E.A., Pastore, M., Prior, T., Herman, G.E., McBride, K.L., 2009. The prevalence of PTEN mutations in a clinical pediatric cohort with autism spectrum disorders, developmental delay, and macrocephaly. Genet. Med. 11 (111–117), 95–103.

Vasa, R.A., Ranta, M., Huisman, T.A., Pinto, P.S., Tillman, R.M., Mostofsky, et al., 2012. Normal rates of neuroradiological findings in children with high functioning autism. J. Autism Dev. Disord. 42, 1662–1670.

Voelbel, G.T., Bates, M.E., Buckman, J.F., Pandina, G., Hendren, R.L., 2006. Caudate nucleus volume and cognitive performance: Are they related in childhood psychopathology? Biol. Psychiatry 60, 942–950.

Volkmar, F., Cook, E.H., Pomeroy, J., Realmuto, G., Tanguay, P., 1999. Practice parameters for the assessment and treatment of children, adolescents, and adults with autism and other pervasive developmental disorders. American Academy of Child and Adolescent Psychiatry Working Group on Quality Issues. J. Am. Acad. Child Adolesc. Psychiatry 38, 32S–54S.

Wechsler, D., 1999. Wechsler Abbreviated Scale of Intelligence. The Psychological Corporation: Harcourt Brace and Company, New York, NY.

Wegiel, J., Kuchna, I., Nowicki, K., Imaki, K., Wegiel, J., Marchi, E., et al., 2010. The neuropathology of autism: defects of neurogenesis and neuronal migration, and dysplastic changes. Acta Neuropathol. 119, 755–770.

Wegiel, J., Schanen, N.C., Cook, E.H., Sigman, M., Brown, W.T., Kuchna, I., et al., 2012. Differences between the pattern of developmental abnormalities in autism associated with duplications 15q11.2-q13 and idiopathic autism. J. Neuropathol. Exp. Neurol. 71, 382–397.

Wolff, J.J., Gu, H., Gerig, G., Elison, J.T., Styner, M., Gouttard, S., et al., 2012. Differences in white matter fiber tract development present from 6 to 24 months in infants with autism. Am. J. Psychiatry 169, 589–600.

World Health Organization, 1992. The ICD-10 Classification of Mental and Behavioural Disorders: Clinical Descriptions and Diagnostic Guidelines. World Health Organization, Geneva.

Wyvell, C.L., Berridge, K.C., 2000. Intra-accumbens amphetamine increases the conditioned incentive salience of sucrose reward: enhancement of reward 'wanting' without enhanced 'liking' or response reinforcement. J. Neurosci. 20, 8122–8130.